Available online at www.sciencedirect.com
SCIENCE DIRECT®
International Journal of Thermal Sciences 43 (2004) 595–610
International Journal of Thermal Sciences
www.elsevier.com/locate/ijts

The numerical modeling of the tube turbulent gas–drop flow with phase changes

V.I. Terekhov *, M.A. Pakhomov

Kutateladze Institute of Thermophysics SB RAS, 1, Acad. Lavrent'ev Avenue, 630090 Novosibirsk, Russia

Received 25 August 2003; accepted 23 November 2003

Available online 27 February 2004

Abstract

Within the concept of heterogeneous-continuum mechanics, the present work numerically, in the two-velocity, two-temperature Euler approximation, examines the turbulent flow of an air–drop mixture through a duct. Effects due to drop evaporation, deposition of drops from the flow onto the duct wall, heat transfer due to direct contacts of drops with the wall, the stochastic motion of drops, and non-isotropic turbulent fluctuations of their velocities on the heat- and mass-transfer processes in the turbulent flow are studied.

Keywords: Heat and mass transfer; Drop evaporation and deposition; Numerical simulation; Turbulent two-phase gas–drop flows

1. Introduction

The mathematical description of gas–drop mixtures with fine drops with allowance for phase transitions is a topical problem both from the theoretical and practical point of view because such flows often occur in nature and found wide application in industry. Examples of natural two-phase flows are given by the drop motion in clouds and mists, and also by the interaction between the atmosphere and ocean. The most important technical applications of such flows include atomization of liquid propellants, protection of working surfaces in engines, and also the use of these flows in power-plant components, in chemical reactors, and in air-conditioning systems.

It should be noted that, normally, relatively small mass concentrations of the liquid component are sufficient for obtaining rather profound intensification phenomena. As a rule, with the mass content of liquid phase in the mixture not exceeding several percents, the heat-transfer intensity can be raised by one order of magnitude. Such effects were observed both for laminar two-phase flows in tubes or around plates (see, e.g., [1,2]) and for turbulent flows (see, e.g., [3–12]).

The mechanism underlying the heat transfer intensification in flows with such heat carriers consists in using the latent heat of vaporization of liquid drops. The drop evaporation depends on a multitude of thermogasdynamic parameters, which fact seriously hampers the theoretical description of combined heat- and mass-transfer processes in ducted gas–drop flows. That is why authors of many numerical studies (see, for instance, [3–5,10,11]) were forced to employ a number of simplifying assumptions; these assumptions did not allow them to develop a rigorous theory of heat- and mass-transfer in two-phase flows even for physically simpler laminar flow mode. With a non-condensing gas present in the mixture, there arises another mechanism, causing additional complications, which governs the vapor diffusion from liquid drops to the vapor–gas mixture; as a result, it becomes necessary to solve interrelated energy and diffusion equations for the vapor–gas mixture [2,3,6,8–11].

The deposition of liquid drops onto the tube wall may have a profound influence on the heat- and mass-transfer processes. Experimental and numerical studies of heat transfer in tube gas–drop flows were reported by [3,12]. A comparison of theoretically predicted wall temperatures with measured ones showed that the intensification of heat transfer between the wall and drops depends on many factors, including the drop concentration, the Reynolds number, and the wall temperature. The local heat transfer coefficient decreases with increasing wall temperature and increasing heat

* Corresponding author.
E-mail address: terekhov@itp.nsc.ru (V.I. Terekhov).

1290-0729/$ – see front matter
doi:10.1016/j.ijthermalsci.2003.11.003

Nomenclature

A $= \pi d^2/4$ drop area cross-cection ..... m^2
B $= \pi d^2$ drop surface area ..... m^2
b_{1D} $= (K_{VS} - K_V)/(1 - K_{VS})$ diffusional injection parameter for the vapor released by an evaporation, which should be found from the saturation curve
C_D coefficient of resistance
$C_f/2$ $= \frac{(\mu+\mu_T)(\partial U/\partial r)_W}{\rho U_{0,m}^2}$ skin friction coefficient
$C_p, C_{pA}, C_{pL}, C_{pV}$ heat capacities of mixture, air, liquid, and vapor ..... $J\cdot kg^{-1}\cdot K^{-1}$
D vapor diffusivity in air ..... $m^2\cdot s^{-1}$
D_{xL}, D_{rL} turbulent diffusivities of drops in the axial and radial directions due to the stochastic motion of drops and their entrainment into the gas flow by intense vortices ..... $m^2\cdot s^{-1}$
d drop diameter ..... m
d_P particle diameter ..... m
$f_{\theta v}$ function that describes the entrainment of liquid drops into the intense pulsations of the gas-phase velocity and the gas-phase temperature
g gravitational acceleration ..... $m\cdot s^{-2}$
g_k, g_ε coefficients of drop entrainment into the micropulsational motion of the gas flow
G mass flow rate ..... $kg\cdot s^{-1}$
G_E mass flow rate from evaporating drop .. $kg\cdot s^{-1}$
J mass flux of vapor from the surface of evaporating drop ..... $kg\cdot(ms)^{-1}$
k turbulent kinetic energy ..... $m^2\cdot s^{-2}$
K_A, K_V mass concentration of air and vapor in binary vapor–air mixture
K_{VS} mass concentration of vapor at the drop surface an evaporating corresponding to saturation parameters at the drop temperature T_L
L heat of vaporization ..... $J\cdot kg^{-1}$
Le $= Pr/Sc$ Lewis number
m $= \rho_L \pi d^3/6$ drop mass ..... kg
M_A, M_V, M_L air, vapor, and liquid mass concentration in the triple air–vapor–drops mixture
n $= \frac{\rho M_{L1}}{\rho_L \pi d_1^3/6}$ numerical density of drops .... m^{-3}
Nu $= \alpha 2R/\lambda$ Nusselt number
Nu_L $= \alpha d/\lambda$ drop Nusselt number
Nu_P $= \alpha_P d_P/\lambda$ Nusselt number non-evaporating particle
P pressure ..... $N\cdot m^{-2}$
Pr $= C_p\mu/\lambda$ Prandtl number
q_E heat spent on evaporation of liquid drops in the flow ..... $W\cdot m^{-2}$
q_F heat spent on heating the vapor–gas flow ..... $W\cdot m^{-2}$
q_W heat flux density supplied to the wall .. $W\cdot m^{-2}$
q_{WF} heat flux density supplied to the gas–vapor–drop flow ..... $W\cdot m^{-2}$
q_{WL} heat flux density due to the conductive heat transfer upon immediate drop/wall contacts ..... $W\cdot m^{-2}$
$\Re$ absolute gas constant ..... $J\cdot mol^{-1}\cdot K^{-1}$
R tube radius ..... m
Re_J $= Jd/\mu$ Reynolds number calculated from the mass rate of the vapor flow from the surface of an evaporating drop
Re_L $= \rho d\sqrt{(U-U_L)^2 + (V-V_L)^2}/\mu$ Reynolds number of disperse phase
Re_T $= k^2/\varepsilon\nu$ turbulence Reynolds number
U, V velocity component in axial and radial directions ..... $m\cdot s^{-1}$
$\langle uv\rangle$ $= -\nu_T \frac{\partial U}{\partial r}$ turbulent stresses in gas phase ..... $m^2\cdot s^{-2}$
$\langle u_L v_L\rangle$ correlations between the longitudinal and transverse pulsating velocities of liquid drops ..... $m^2\cdot s^{-2}$
ΔU $= U - U_L$ relative velocity of the two phases ..... $m\cdot s^{-1}$
$\langle u^2\rangle, \langle v^2\rangle$ root–mean–square velocity fluctuations in axial and radial directions ..... $m^2\cdot s^{-2}$
U_* wall friction velocity ..... $m\cdot s^{-1}$
Sc $= \nu/D$ Schmidt number
Sh $= \beta d/D$ Sherwood number
St_D $= -\rho_V D \frac{\partial K_V^*}{\partial r}/\rho U(K_V^* - K_V)$ diffusional Stanton number
T, T_L mixture and drop temperatures ..... K
$\langle tv\rangle$ $= -\frac{\nu_T}{Pr_T}\frac{\partial T}{\partial r}$ turbulent heat flux in gas phase ..... $K\cdot m\cdot s^{-1}$
t amplitude of gas-temperature pulsations .... K
Tu turbulence intensity in the flow
V_{LW} drop deposition velocity ..... $m\cdot s^{-1}$
V_+^{TP} dimensionless turbophoresis velocity
W $= (1+Re_L^{2/3}/6)$ correction factor for the Stokes law
We $= \rho|\vec{U} - \vec{U}_L|d_1/\sigma$ Weber number
y coordinate normal to the wall ..... m

Greek symbols

α heat transfer coefficient ..... $W\cdot m^{-2}\cdot K^{-1}$
β mass transfer coefficient ..... $m\cdot s^{-1}$
δ boundary layer thickness ..... m
ε dissipation rate of turbulent kinetic energy ..... $m^2\cdot s^{-3}$
Φ volume mass concentration of drops
Γ^E $= \nu_T/\langle u^2\rangle$ is the geometric scale of the phase-carrier turbulence ..... m

λ	thermal conductivity	$\mathrm{W\cdot m^{-1}\cdot K^{-1}}$
μ	dynamic viscosity	$\mathrm{N\cdot s\cdot m^{-2}}$
μ_T	eddy viscosity	$\mathrm{N\cdot s\cdot m^{-2}}$
ν	kinematic viscosity	$\mathrm{m^2\cdot s^{-1}}$
Θ	relative temperature profile	
$\langle\theta v_L\rangle$	correlation between the drop-temperature fluctuations and drop-velocity fluctuations	$\mathrm{K\cdot m\cdot s^{-1}}$
Ω^{ε}	$=(15\nu/\varepsilon)^{1/2}$ time microscale	s
Ω^{E}	Eulerian time macroscale	s
Ω^{L}	Lagrangian time macroscale	s
$\Omega^{\varepsilon L}$	time of particle interaction with the intense vortices	s
$\Omega_{\theta u}$	time of drop contact with intense gas-temperature pulsations	s
ρ, ρ_L, ρ_V	mixture, liquid, vapor densities	$\mathrm{kg\cdot m^{-3}}$
σ	surface tension	$\mathrm{N\cdot m^{-1}}$
τ	$=\rho_L d^2/(18\mu W)$ particle relaxation time	s
τ_{Θ}	$=C_{pL}\rho_L d_L^2/(6\lambda Nu_L)$ particle thermal relaxation time	s

Subscripts

0	parameter at the duct axis
1	parameter under inlet conditions
A	air
C	critical value of a parameter
D	diffusional parameter
i	current calculation cross-section along the axial direction
$i-1$	previous calculation cross-section along the axial direction
L	drop
m	mean-mass parameter
P	non-evaporating particle
T	turbulent parameter
V	vapor
W	parameter under condition at the wall
$*$	parameter under saturation condition
$+$	denotes the dimensionless variables in dynamic universal units

flux density, and it increases with increasing flow velocity and increasing concentration of liquid drops.

The case of heat and mass transfer in ducted turbulent vapor–gas–drop flow was considered by Terekhov and Pakhomov [9]. To model the turbulent structure of the gas phase, the k–ε model of turbulence was used, modified to the case of a flow with liquid drops. It was assumed that the drops do not affect the flow velocity profile. Additionally, the drop size was assumed to be uniform along the duct radius due to intense turbulent mixing of drops, although it continuously decreased along the duct length due to evaporation processes. The numerical concentration of the dispersed phase remained fixed throughout the whole flow region excluding some decrease in the total number of liquid drops caused by their deposition onto the duct well. The rate of the latter process was calculated by the model proposed by [13], irrespectively of the transfer equations for the gas phase. Accordingly, the time-averaged and pulsational equations of motion for the dispersed phase were excluded from the system of governing equations, which approximation was rather crude. Nevertheless, for low initial mass concentrations of liquid drops ($M_{L1} \leqslant 5\%$) and for relatively small particles ($d_1 \leqslant 100$ μm) this approach, as it was shown by [9], was capable of providing a good agreement with the experiment, proving the adequacy of the model to real flows under the indicated conditions.

The statement of the problem in the present study was based on using a unified system of Euler equations for transport phenomena in the gas and dispersed phases. The adopted approach takes into account the effect of turbulent migration of liquid drops on the rate of the gas flow, on the intensity of heat and mass transfer in it, on the turbophoretic force, and on the diffusion of particles caused by gradients of their concentration. On the whole, the equations for the mean drop velocity and for its root–mean–square fluctuations comply with those used by Shraiber et al. [14], Nigmatulin [15]; Volkov et al. [16], and Derevich [17]. The main purpose of the present study was to compare the numerical data obtained under the assumption of constancy of numerical concentration of drops and their ideal mixing, with the data predicted by the model of interpenetrating continua in terms of Euler variables.

In the present study, a great number of factors, influencing the heat and mass transfer, such as the deposition of liquid drops onto the duct wall, the effect of drop evaporation in the flow and on the duct wall, and the pulsational motion of liquid drops across the duct were taken into account. Data obtained during testing the model are described, and a comparison between the numerical and experimental results of different authors is given.

2. Physical model

We consider the hydrodynamics and heat and mass transfer in a turbulent gas–vapor–drop flow through a pipe. The consideration takes into account the drop evaporation, the interaction between the phases, the deposition of drops onto the wall, the heat-transfer between the drops and the wall, the turbulent motion of liquid drops, the turbophoresis, and the vapor diffusion into the vapor–gas mixture. The radiative heat transfer was ignored because it was weak (see, for instance, [2–11]). Next, we assumed that, as drops come into contact with the wall, they undergo instantaneous evaporation; for this reason, the duct wall was assumed to always remain dry. To take into account the conductive heat transfer due to direct contacts of drops with the wall, we used the model of Mastanaiah and Ganic [3]. We consider

the following three-stage mechanism of heat transfer in the two-phase flow:

(1) part of the heat supplied to the wall is transferred to drops deposited onto the wall to be subsequently spent on their evaporation;
(2) part of the heat supplied to the wall is transferred to the gas–vapor–drop mixture;
(3) part of the heat supplied to the vapor–gas mixture is transferred to the liquid drops to be subsequently spent on their heating and evaporation.

The volume concentration of the liquid phase is low ($\Phi < 10^{-4}$), and the drops are small (their diameter d_1 is smaller than 100 μm). In the zones where drops evaporate completely, their numerical concentration is modeled with zero-diameter particles. In the flow, no coalescence of liquid drops into larger drops and no drop defragmentation occur. According to [3], the Weber number calculated from the difference between the velocities of the two phases and from the drop size, $We = \rho|\vec{U} - \vec{U}_L|d_1/\sigma \ll 1$, is much lower than the critical Weber number $We_C \approx 7$. All drops are shaped as spheres with static boundaries. According to [16,18], in a ducted flow of a two-phase mixture the effect due to interparticle collisions can be neglected if the volume concentration Φ_L of the dispersed phase is lower than 0.1%. The drop temperature was assumed uniform along the drop radius.

To simplify the computational model, we used the assumption that the vapor evaporated from drop surfaces has no effect on the kinetic-energy profiles of the gas-phase turbulence and on the dissipation rate of the kinetic energy.

3. Mathematical model

3.1. Gas phase

With the adopted assumption, for the axisymmetric case of a two-phase gas–drop flow in the boundary-layer approximation, the system of governing equation, which includes the continuity equation, the equation of motion in the axial direction, the energy equation, and the equation of vapor diffusion into the binary vapor–gas mixture has the form:

$$\frac{\partial U}{\partial x} + \frac{1}{r}\frac{\partial (rV)}{\partial r} = \frac{6J\Phi}{\rho d}$$

$$\rho\left[U\frac{\partial U}{\partial x} + \frac{V}{r}\frac{\partial (rU)}{\partial r}\right] = -\frac{\partial P}{\partial x} + \frac{1}{r}\frac{\partial}{\partial r}\left[r(\mu + \mu_T)\frac{\partial U}{\partial r}\right] - \frac{3}{4d}C_D\rho\Phi(U - U_L)\left|\vec{U} - \vec{U}_L\right| \pm \rho g$$

$$\rho C_p\left[U\frac{\partial T}{\partial x} + \frac{V}{r}\frac{\partial (rT)}{\partial r}\right] = \frac{1}{r}\frac{\partial}{\partial r}\left[r\left(\frac{\mu}{Pr} + \frac{\mu_T}{Pr_T}\right)\frac{\partial T}{\partial r}\right] - \alpha nB(T - T_L) + \rho D_T\frac{\partial K_V}{\partial r}(C_{pV} - C_{pA})\frac{\partial T}{\partial r}$$

$$\rho\left[U\frac{\partial K_V}{\partial x} + \frac{V}{r}\frac{\partial (rK_V)}{\partial r}\right] = \frac{1}{r}\frac{\partial}{\partial r}\left[r\left(\frac{\mu}{Sc} + \frac{\mu_T}{Sc_T}\right)\frac{\partial K_V}{\partial r}\right] + JnB$$

$$\rho = P/(\Re T), \qquad \partial P/\partial r = 0 \tag{1}$$

Here ρ, λ, μ, and D are the density, the thermal conductivity, and the dynamic viscosity of the air–vapor flow, and the coefficient of vapor molecular diffusion into the gas; C_p, C_{pA}, and C_{pV} are the specific heat capacities of the mixture, air, and vapor; $A = \pi d^2/4$ is the cross-sectional area of a drop; $B = \pi d^2$ is the surface area of a drop; T and T_L are the mixture temperature and the drop temperature; $n = \frac{6\rho M_{L1}}{\rho_L \pi d_1^3}$ [m^{-3}] is the numerical concentration of liquid drops in the pipe; $J = \rho_V W_V$ is the mass flux of the vapor from the surface of an evaporating drop [$\mathrm{kg\cdot m^{-2}\cdot s^{-1}}$]. The subscripts A, L, and V refer to air, drop, and vapor. The subscript T denotes turbulent characteristics.

The continuity, energy, and diffusion equations contain source and sink terms that model the effect of liquid drops on transfer processes, and the equation of motion involves an additional term that takes into account the dynamic interaction between the phases.

At the initial section of the pipe, the relation for determining the derivative $\partial P/\partial x$, which enters the equation of motion, is represented by the Bernoulli integral with allowance for the additional inflow of vapor mass due to drop evaporation:

$$-\frac{\partial P}{\partial x} = \rho U_0\frac{\partial U_0}{\partial x} + JnB\left|\vec{U} - \vec{U}_L\right|$$

The change of the flow velocity in the undisturbed core of the flow can be found from the equation of constancy of the mass flux passing the cross-section of the duct:

$$\rho U_0\pi(R - \delta)^2 + 2\rho\pi\int_{R-\delta}^{R} Ur\,\mathrm{d}r = G_1 + G_E \tag{2}$$

where δ is the boundary-layer thickness; $G_1 = \rho U_m\pi R^2(1 - M_L)$—the mass rate of the vapor–gas mixture flow in the current duct cross-section; $G_E = \rho_V U_m\pi R^2(M_{Vi} - M_{Vi-1})$—the mass rate due to droplets vaporization; U_m is the mass-mean flow velocity.

The final expression for the flow velocity U_0 at the pipe axis can be written as follows:

$$U_0 = \frac{G_1 + G_E - 2\rho\pi\int_{R-\delta}^{R} Ur\,\mathrm{d}r}{\rho\pi(R - \delta)^2}$$

The turbulent stress, the heat flux, and the turbulent viscosity μ_T were calculated within the framework of the two-parametric k–ε model:

$$\langle uv\rangle = -\nu_T\frac{\partial U}{\partial r}$$

$$\langle tv\rangle = -\frac{\nu_T}{Pr_T}\frac{\partial T}{\partial r}$$

$$\mu_T = C_\mu f_\mu \rho k^2/\varepsilon$$

3.2. Two-parametric model of turbulence

The equations for the kinetic turbulence energy k and for the dissipation rate of this energy ε modified to the case of a flow with a dispersed phase are

$$\rho\left[U\frac{\partial k}{\partial x}+\frac{V}{r}\frac{\partial(rk)}{\partial r}\right] = \frac{1}{r}\cdot\frac{\partial}{\partial r}\left[r\left(\mu+\frac{\mu_T}{\sigma_k}\right)\frac{\partial k}{\partial r}\right]+Y-\rho\varepsilon+S_k$$

$$\rho\left[U\frac{\partial \varepsilon}{\partial x}+\frac{V}{r}\frac{\partial(r\varepsilon)}{\partial r}\right] = \frac{1}{r}\cdot\frac{\partial}{\partial r}\left[r\left(\mu+\frac{\mu_T}{\sigma_\varepsilon}\right)\frac{\partial \varepsilon}{\partial r}\right] + \frac{C_{\varepsilon 1}\varepsilon f_1 Y}{k}-\frac{C_{\varepsilon 2}\varepsilon^2\rho f_2}{k}+S_\varepsilon \tag{3}$$

The following constants and damping functions were adopted by [19]: $C_\mu = 0.09$, $\sigma_k = 1.4$, $\sigma_\varepsilon = 1.3$,

$$C_{\varepsilon 1}=1.45,\qquad C_{\varepsilon 2}=1.9,\qquad f_1=1$$

$$f_2=\left[1-\exp(-y_+/6)\right]^2\left[1-0.3\exp\left\{-\left(Re_T^{3/4}/6.5\right)^2\right\}\right]$$

$$f_\mu=\left[1-\exp(-y_+/26)\right]^2\left(1+4.1/Re_T^{3/4}\right)\quad\text{and}$$

$$Y=\mu_T\left(\frac{\partial U}{\partial r}\right)^2$$

where $Re_T = k^2/\varepsilon\nu$ is the turbulent Reynolds number.

The first item in right side determine the additional dissipation of gas stream turbulence due to pulsating interfacial slip. The second item describe the energy transfer with averaged motion of the gas phase, caused by the averaged interfacial slip with non-homogeneous distribution of dispersed phase concentration [16]:

$$S_k=-\frac{2M_L\rho k}{\tau}\exp\left(-\Omega^L/\tau\right)-g_k\mu_T(U-U_L)\frac{\partial U}{\partial x}\frac{\partial M_L}{\partial x}$$

The first term connected with small particle influence on the velocity of dissipation of turbulence energy of the flow due to pulsating interfacial slip. The second item describe the influence on the turbulence of averaged slip and the non-homogeneous distribution of droplets [16]:

$$S_\varepsilon=-\frac{2M_L\rho_L\varepsilon}{\tau}\exp\left(-\Omega^\varepsilon/\tau\right)+\frac{2}{3}g_\varepsilon\rho\varepsilon\left[(U-U_L)\frac{\partial M_L}{\partial x}+(V-V_L)\frac{\partial M_L}{\partial r}\right]$$

The coefficients of drop entrainment into the micropulsational motion of the gas flow in the above relations are given by the formulas

$$g_k=\Omega^{\varepsilon L}/\tau-1+\exp\left(-\Omega^{\varepsilon L}/\tau\right)\quad\text{and}$$

$$g_\varepsilon=\Omega^{\varepsilon}/\tau-1+\exp\left(-\Omega^{\varepsilon}/\tau\right)$$

The values of turbulent Prandtl and Schmidt numbers were assumed spatially uniform both along the pipe length and pipe radius, and also equal to each other, $Pr_T = Sc_T = 0.9$. The Lewis number was taken equal to unity: $Le = Pr/Sc = 1$.

3.3. Momentum and energy equation for the drops

Numerous present-day studies show that the main forces acting on a particle in a turbulent flow under the conditions under consideration are the turbophoresis, the drag, and the gravity force. The Saffman force is not considered because its exact value for turbulent flows is unknown. DNS and LES data obtained by Uijetterwaal and Oliemans [20] show that the predominant influence on the motion of particles is exerted by the turbulence and by the inertial forces. The thermophoretic effect and the Magnus force are ignored because both are weak. The aerodynamic forces due to the pressure gradient, the attached mass and the Basset effect are assumed weak since their order is proportional to the gas–liquid density ratio; in the majority of practical cases, this ratio approximately equals 10^{-3}.

The system of the continuity equation, the equation for the mean velocity of the dispersed flow, and the continuity equation in the cylindrical coordinate system has the form [17]:

$$\frac{\partial(\Phi U_L)}{\partial x}+\frac{1}{r}\frac{\partial(r\Phi V_L)}{\partial r}=-\frac{6(J+\rho_L V_{LW})\Phi}{\rho_L d}$$

$$U_L\frac{\partial U_L}{\partial x}+\frac{V_L}{r}\frac{\partial(rU_L)}{\partial r}+\frac{\partial\langle u_L^2\rangle}{\partial x}+\frac{1}{r\Phi}\frac{\partial}{\partial r}\left[r\Phi\langle u_L v_L\rangle\right] = \frac{U-U_L\pm\tau g}{\tau}-\frac{D_{xL}}{\tau}\frac{\partial\ln\Phi}{\partial r}$$

$$U_L\frac{\partial V_L}{\partial x}+\frac{V_L}{r}\frac{\partial(rV_L)}{\partial r}+\frac{\partial\langle v_L^2\rangle}{\partial r} = \frac{U-U_L}{\tau}-\frac{D_{rL}}{\tau}\frac{\partial\ln\Phi}{\partial r} \tag{4}$$

Here V_{LW} is the rate of drop deposition onto the duct wall, and $\langle u_L v_L\rangle$ are the correlations between the longitudinal and transverse pulsating velocities of liquid drops, representing turbulent stresses in the dispersed phase and written according to Derevich [17]:

$$\langle u_L v_L\rangle = q_L\langle uv\rangle-\frac{1}{2}\tau\langle v_L^2\rangle\frac{\partial U_L}{\partial r}$$

$$D_{xL}=\tau\left(\langle u_L^2\rangle+p_L\langle u^2\rangle\right)$$

$$D_{rL}=\tau\left(\langle v_L^2\rangle+p_L\langle v^2\rangle\right)$$

The functions that describe the entrainment of drops into the turbulent motion of the phase-carrier are [21]:

$$q_L=1-\exp\left(-\Omega^{\varepsilon L}/\tau\right),\qquad p_L=\Omega^{\varepsilon L}/\tau-q_L$$

The energy equation for the mean drop temperature is

$$U_L\frac{\partial T_L}{\partial x}+\frac{V_L}{r}\frac{\partial(rT_L)}{\partial r}+\frac{1}{r\Phi}\frac{\partial}{\partial r}\left(r\Phi\langle\theta v_L\rangle\right) = \frac{6}{C_{pL}\rho_L d}\left\{\alpha(T-T_L)-J\left[L+C_{pV}(T-T_L)\right]\right\} \tag{5}$$

where $\langle\theta v_L\rangle$ is the correlation between the drop-temperature fluctuations and drop-velocity fluctuations, which was calculated by the following formula proposed by [17]:

$$\langle\theta v_L\rangle = f_{\theta v}\langle tv\rangle - \left(\frac{1}{\tau} - \frac{1}{\tau_\Theta}\right)^{-1}\langle v_L^2\rangle\frac{\partial T_L}{\partial r} \tag{6}$$

Here t is the amplitude of gas-temperature pulsations and $f_{\theta v}$ is the function that describes the entrainment of liquid drops into the intense pulsations of the gas-phase velocity and the gas-phase temperature; this function has the form

$$f_{\theta v} = \left\{\tau\left[1-\exp(-\Omega_{\theta u}/\tau)\right] + \tau_\Theta\left[1-\exp(-\Omega_{\theta u}/\tau_\Theta)\right]\right\}(\tau+\tau_\Theta)^{-1}$$

where $\Omega_{\theta u}$ is the time during which drops contact with intense gas-temperature pulsations. In a first-order approximation, we assume that $\Omega_{\theta u} \approx \Omega^{\varepsilon L}$ ($\Omega^{\varepsilon L}$ is the time of particle interaction with the intense vortices).

It should be noted that the turbulent transfer of heat by the dispersed phase in Eq. (6) is caused by the involvement of drops into intense gas-phase velocity and gas-phase temperature pulsations, and also by the heat flux transferred in the radial direction by the stochastic motion of liquid drops [17].

The time during which drop contacts intense vortices is given by the following formula [21]:

$$\Omega^{\varepsilon L} = \begin{cases} \Omega^E, & \left|\vec{U}-\vec{U}_L\right|\Omega^E \leqslant \Gamma^E \\ \Gamma^E/\left|\vec{U}-\vec{U}_L\right|, & \left|\vec{U}-\vec{U}_L\right|\Omega^E > \Gamma^E \end{cases}$$

where $\Omega_{\theta u}$ is the time of drop contact with intense gas-temperature pulsations. In a first-order approximation, we assume that $\Omega_{\theta u} \approx \Omega^{\varepsilon L}$.

3.4. Pulsational equation for the dispersed-phase velocity

The second moments of the turbulent fluctuations of drop velocity in the longitudinal and transverse directions can be found from the following equations [17]:

$$\begin{aligned} &U_L\frac{\partial\langle u_L^2\rangle}{\partial x} + \frac{V_L}{r}\frac{\partial(r\langle u_L^2\rangle)}{\partial r} + \frac{1}{r\Phi}\frac{\partial}{\partial r}\left[\frac{\partial(r\Phi\langle u_L^2 v_L\rangle)}{\partial r}\right] + 2\langle u_L^2\rangle\frac{\partial U_L}{\partial x} \\ &\quad = \frac{2}{\tau}\left(q_L\langle u^2\rangle - \langle u_L^2\rangle\right) \\ &U_L\frac{\partial\langle v_L^2\rangle}{\partial x} + \frac{V_L}{r}\frac{\partial(r\langle v_L^2\rangle)}{\partial r} + \frac{1}{r\Phi}\frac{\partial}{\partial r}\left[\frac{\partial(r\Phi\langle v_L^3\rangle)}{\partial r}\right] \\ &\quad = \frac{2}{\tau}\left(q_L\langle v^2\rangle - \langle v_L^2\rangle\right) \end{aligned} \tag{7}$$

The third moments of velocity pulsations describe the diffusion flux of energy due to the stochastic motion of drops in the axial and radial directions Derevich [17]:

$$\begin{aligned} \langle v_L^2 v_L\rangle &= -\frac{\tau\langle v_L^2\rangle}{3}\frac{\partial\langle u_L^2\rangle}{\partial r} \\ \langle v_L^3\rangle &= -\tau\langle v_L^2\rangle\frac{\partial\langle v_L^2\rangle}{\partial r} \end{aligned} \tag{8}$$

It follows from (8) that the transfer of energy by the stochastic motion of drops is determined by the intensity of drop velocity pulsations in the transverse direction and by the gradient of corresponding second moments.

3.5. Drag and heat and mass transfer of an individual evaporating drop

For evaporating drops, the drag coefficient C_D is given by the following expression [3]:

$$C_D = \frac{C_{DP}}{1 + C_p(T-T_L)/L}$$

Here C_{DP} is the drag coefficient of non-evaporating drops, which can be calculated from the relations proposed by Volkov et al. (1994)

$$C_{DP} = \begin{cases} 24/Re_L, & Re_L < 1 \\ \frac{24}{Re_L}\left(1 + Re_L^{2/3}/6\right), & Re_L \geqslant 1 \end{cases}$$

The conservation equation for the vapor mass on the surface of an evaporating drop can be written as

$$J = \underbrace{JK_{VS}}_{\text{I}} - \underbrace{\rho_V D\left(\frac{\partial K_V}{\partial r}\right)_{\text{drop}}}_{\text{II}} \tag{9}$$

where K_{VS} is the vapor concentration at the interface between the vapor–gas mixture and the drop, which should be taken at saturation parameters for the drop temperature T_L;

(I) is the convective (Stefan) flux of the mass of vapor; and
(II) is the mass rate of the vapor due to concentration gradients.

Taking into account that the diffusional Stanton number St_D has the form

$$St_D = -\rho_V D\frac{\partial K_{VS}}{\partial r}/\rho\left(\vec{U}-\vec{U}_L\right)(K_{VS}-K_V)$$

we can write the equation of mass conservation [9] in the form

$$J = St_D\rho\left(\vec{U}-\vec{U}_L\right)b_{1D} \tag{10}$$

Within the framework of the film model, the effect of the transverse flow of mass on the heat- and mass-transfer coefficients of evaporating drops can be described by the following relations [22]:

$$Nu_L = \frac{Re_J Pr}{\exp(Re_J Pr/Nu_P) - 1}$$

$$Sh_L = \frac{Re_J Pr}{\exp(Re_J Pr/Sh_P) - 1}$$

where Nu_P and Sh_P are the Nusseldt and Sherwood numbers for non-evaporating drops:

$$Nu_P = \alpha_P d/\lambda = 2 + 0.6\,Re_L^{1/2}Pr^{1/3} \quad \text{and}$$

$$Sh_P = \beta d/D = 2 + 0.6\,Re_L^{1/2}Sc^{1/3}$$

Here $Re_L = d\sqrt{(U-U_L)^2+(V-V_L)^2}/\nu$ is the particle Reynolds number calculated from the slip velocity of the two phases.

The diffusional Stanton number can be found from the expression

$$St_D = Sh_L/(Re_L Sc) \tag{11}$$

as a result, Eq. (11) with allowance for [10] acquires the form

$$J = \left(2 + 0.6\,Re_L^{1/2} Sc^{1/3}\right)\rho\left(\vec{U}-\vec{U}_L\right)b_{1D}/(Re_L Sc) \tag{12}$$

According to [23], the heat-transfer coefficient α of evaporating drops is related to the analogous coefficient α_P of non-evaporating drops by the formula

$$\alpha = \frac{\alpha_P}{1 + C_p(T-T_L)/L}$$

The material-balance equation for a binary air–vapor mixture is

$$K_A + K_V = 1$$

For a ternary vapor–gas–liquid mixture, this equation can be written as

$$M_A + M_V + M_L = 1 \tag{13}$$

The relation between the mass concentrations K and M of the mixture components is given by the formulas

$$K_V = M_V/(M_A + M_V) \quad \text{and}$$
$$K_A = M_A/(M_A + M_V) = 1 - K_V$$

The expression for the current drop diameter in the ith calculation section is

$$d_{i,j}^3 = d_{i-1,j}^3 - J d_{i-1}^2 \frac{6\Delta x}{\rho_L U_{i,j}} \tag{14}$$

Under intense evaporation processes, as the flow moves in the pipe, the gas-phase velocity increases due to vaporization. This process is described by the source term in the continuity equation. Here, the increase in the local values of the flow velocity over the pipe cross-section depends on the gas-phase temperature field. The rate-mean velocity of the vapor–gas mixture was calculated with due consideration for the inflow of vapor mass from evaporating drops.

3.6. Heat transfer of drops deposited onto the duct wall

As liquid drops precipitate on the wall, part of the heat flux goes into their evaporation. As in the majority of previous models, for instance, in the models used by Ganic and Rohsenow [24] and [3], the possibility of superposition of heat fluxes was assumed in the present study. The heat-flux density q_W supplied to the pipe wall consists of the heat to be subsequently transferred from the wall to drops (q_{WL}) and the heat transferred from the wall to the vapor–gas–drop mixture (q_{WF}).

The density of the flux of heat from the wall to the deposited drops is given by the following formula [24]:

$$q_{WL} = \exp\left[1 - (T_W/T_L)^2\right] V_{LW}\rho_L L M_{Lm} \tag{15}$$

The mass-mean concentration of drops over the pipe cross-section is given by the formula

$$M_{Lm} = \frac{2}{U_m R^2}\int_0^R M_L U r\,\mathrm{d}r$$

To determine the mass concentration M_{LW} of drops deposited onto the duct wall from the turbulent gas–vapor–drop flow, we used the following algebraic relations [9]. The mass of the liquid precipitating onto the duct wall is

$$m_W = \rho_L V_{LW}\Delta x 2\pi\,\Delta r\,\Delta t$$

where Δx and Δr are the steps along the longitudinal and transverse coordinates, and Δt is the time interval.

The numerical concentration of the dispersed phase in the flow of precipitating drops is

$$n_W = \frac{6m_W}{\pi^2\rho_L d^3 R^2\Delta x}$$

The mass concentration of the drops precipitating onto the wall surface is

$$M_{LW} = \frac{n_W\rho_L\pi d^3}{6\rho} \tag{16}$$

3.7. Determination of the intensity of gas-phase pulsations

To perform a comparison of numerical results with experimental data on the components of gas-phase velocity pulsations and drop velocity pulsations, it was necessary to calculate these quantities. It was assumed that the drops are relatively large, so that the dynamic time τ of their relaxation is longer than the integral Euler time scale Ω^E of the turbulence.

The time macroscale of the flow-core turbulence was calculated from the relation borrowed from the work of Simonin et al. [25]:

$$\left(\Omega^E\right)_0 = 0.22k/\varepsilon$$

Near the duct wall, the integral Euler time scale of the turbulence, needed for determining the transverse component of gas-phase pulsations, was approximated by the following relation [17]:

$$\Omega_+^E = \Omega^E U_*/\nu = \sqrt{\left(\Omega_+^E\right)_0^2 + \left(\Omega_+^E\right)_W^2}, \qquad \left(\Omega_+^E\right)_W \approx 10$$

The radial component of the root–mean–square gas-phase velocity pulsations is related with the turbulent diffusivity:

$$\left\langle v^2\right\rangle = \nu_T/\Omega^L$$

The amplitude of gas-phase velocity pulsations in the axial direction was calculated by the following formula (see Derevich [17]):

$$\left\langle u^2\right\rangle \approx 1.3k$$

and the relation between the time scales of turbulence for the case of small particles has the form

$$\Omega^L \approx 0.608\Omega^E$$

4. Inlet and boundary conditions

At the pipe axis and at the external border of the boundary layer, the following symmetry conditions were set:

$$\frac{\partial T}{\partial r} = \frac{\partial K_V}{\partial r} = \frac{\partial U}{\partial r} = V = \frac{\partial U_L}{\partial r} = V_L = \frac{\partial \langle u_L^2 \rangle}{\partial r} = \frac{\partial \langle v_L^2 \rangle}{\partial r} = \frac{\partial T_L}{\partial r} = \frac{\partial k}{\partial r} = \frac{\partial \varepsilon}{\partial r} = 0 \tag{17}$$

At the duct wall, no-slip and impermeability conditions were assumed. The boundary condition for the heat flux is $q_W = \text{const}$:

$$U = V = \frac{\partial K_V}{\partial r} = 0, \qquad -\lambda \frac{\partial T}{\partial r} = q_{WF}$$

$$k = 0, \qquad \varepsilon_W = \nu \left(\frac{\partial^2 k}{\partial r^2} \right)_W \tag{18}$$

The boundary conditions for squared fluctuations of the axial and radial velocities, and for squared fluctuations of the dispersed-gas temperature are [17]:

$$\langle v_L^2 \rangle \frac{\partial U_L}{\partial r} = -\frac{2}{\tau} q_L \nu_T \left(\frac{\partial U}{\partial r} \right)_W$$

$$V_{LW} = \left(\frac{2}{\pi} \langle v_L^2 \rangle \right)^{1/2}$$

$$\frac{\partial \langle u_L^2 \rangle}{\partial r} = 0$$

$$\frac{\partial \langle v_L^2 \rangle}{\partial r} = -V_{LW}/\tau \tag{19}$$

$$\left(\frac{1}{\tau} - \frac{1}{\tau_\Theta} \right)^{-1} \langle v_L^2 \rangle \frac{\partial T_L}{\partial r} = f_{\theta v} \langle tv \rangle_W \tag{20}$$

At the inlet section of the duct, a uniform distribution of the temperatures and velocities of the phases was assumed. All drops at the duct inlet were assumed to have identical sizes and temperatures. At the inlet, either identical or different temperatures of the phases could be adopted (equilibrium and non-equilibrium regimes).

$$U = U_1, \qquad V = V_1, \qquad T = T_1$$

$$M_L = M_{L1}, \qquad T_L = T_{L1}, \qquad d = d_1$$

$$K_V = K_{V1}, \qquad k = k_1, \qquad \varepsilon = \varepsilon_1 \tag{21}$$

For uniform inlet profiles of the turbulent energy k and for the rate of its dissipation ε, the data of [26] were used:

$$k_1 = 1.5 Tu^2 U_1^2, \qquad \varepsilon_1 = C_\mu \frac{k_1^{3/2}}{0.06R}$$

The turbulence degree Tu of the gas phase at the inlet to the duct assumed to equal 4%, and that in the viscous sublayer, 6%.

Relations (1)–(16) with corresponding boundary and initial conditions (17)–(21) provide a closed system of equations governing the heat- and mass-transfer processes in a turbulent two-phase flow. This system makes it possible to calculate all sought quantities, including the temperature field and the distributions of the concentrations of phases and components of the vapor–gas mixture, and also to reveal the evolution of drop sizes in the downstream direction.

5. Numerical algorithm

The numerical solution of the parabolic partial equations was obtained with the help of the Crank–Nicholson finite-difference scheme reported by [27], by transforming the initial system of differential equations into a system of discrete linear algebraic equations. The obtained tridiagonal system was solved by the sweep method using the Thomas algorithm, which was described in detail by [27]. A calculation grid with densening of nodal points in the direction towards the wall was used to resolve the details of the turbulent flow in the near-wall zone. In the longitudinal direction, the grid was uniform.

Since the step of the calculation grid was non-uniform in the radial direction, we applied a transform of the coordinate r making it possible to solve the equations on a spatially uniform grid. The transform of coordinates reported by [27] is quite appropriate for solving the two-dimensional boundary-layer problem.

All calculations were performed on a grid with 101 nodal points in the longitudinal direction and with 101 nodal points in the radial direction. In addition, methodical calculations were performed on a smaller, nested grid; this grid had 201 nodal points over the pipe length and 201 nodal points over the pipe radius. Further increase in the number of nodal points yielded no substantial changes in the calculation results.

Since the system (1)–(21) included non-linear equations, an iteration procedure was used to calculate its solution. The convergence criteria $|Y_i - Y_{i-1}| < 10^{-4}$, where Y stands for U, k, ε, T, K_V, U_L, V_L, $\langle u_L^2 \rangle$, $\langle v_L^2 \rangle$, and T_L, were adopted. The calculations were terminated if all these criteria were met.

6. Testing of the model

6.1. Single-phase regime of the gas flow

The adopted model was tested by comparing its predictions with the data obtained by means of Direct Numerical Simulations, and also with the PIV and LDA data obtained by Eggels et al. [28] for a tube single-phase isothermal air flow. In addition, a good agreement was obtained between the results yielded by the present k–ε model and the heat-transfer regularities in the turbulent single-phase flow [29,30].

6.2. Two-phase flow of an air–drop mixture without heat transfer

To perform a comparative analysis of the two-phase flow mode, the experimental data of Varaksin [31] for a descend-

ing gas–glass particle flow were used. The calculated and measured distributions of the velocities of the phases over the pipe radius are shown in Fig. 1. The initial data for the calculations were: $2R = 46$ mm, $Re = 12\,300$, $U_0 = 4$ m·s^{-1}, $M_P = 2\%$, $d = 50$, 100 μm, $\rho_p = 2550$ kg·m^{-3}, and $\tau_+ = 79$.

Close consideration of the data of Fig. 1 for the two-phase flow with a low concentration of the dispersed phase shows a good agreement between the predicted and measured values throughout the whole flow region examined in this study. The velocity of glass particles is higher than the gas-flow velocity, and the difference between the velocities increases in the direction towards the duct wall, which can be explained by considerable inertia of glass particles. Both the calculation and experimental data are indicative of an increase in the slip velocity of the phases in the near-wall region of the descending flow. It should be noted that the data yielded by the model qualitatively comply with the Large Eddy Simulation results reported by [20] for a vertical isothermal dispersed flow through a cylindrical channel.

The radial distributions of relative axial and radial pulsating velocities of the gas and dispersed phases are compared in Fig. 2 with the experimental data reported by [31]. The experiments were performed for a descending air–glass particle flow using the LDA technique. The initial data for the numerical experiment were as follows: $2R = 46$ mm, $U_0 = 5.2$ m·s^{-1}, $d = 50$ μm, $\rho_p = 2550$ kg·m^{-3}, $M_P = 5\%$, $\tau_+ = 125$, and $Re = 15\,300$.

The comparison allows the following conclusions to be made. The predicted intensities of gas-phase and glass-particle pulsations in the longitudinal and transverse directions compare well with the experimental data. A satisfactory agreement between the pulsational characteristics of the particles predicted by the model of [17] and the experimental data of [31] is worth noting. The calculation results agree better with experimental data when considering transverse pulsations of the phase-carrier velocity, probably because of the chosen approximation for $\langle u^2 \rangle$. The amplitude of turbulent pulsations of particle velocity in the axial direction is appreciably higher than in the radial direction. This phenomenon is caused not only by the fact that the pattern of the gas-phase turbulence is non-isotropic, but also by the additional generation of turbulence by particles as the particles move in the field of the dispersed-phase axial velocity gradient. It is seen from the distributions shown in Fig. 2 that the intensity of transverse particle velocity pulsations is lower than the corresponding value for the phase-carrier. This finding can be explained as follows. The Stokes number in the large-scale pulsational motion is defined as $Stk = \tau/\Omega^L$, which yields $Stk \approx 1$; it follows from here that particles readily get entrained into the large-scale pulsational motion and easily take off energy from the turbulent phase-carrier eddies. A decrease in the intensity of transverse pulsations of the gas phase suppresses the pulsations of fine particles; this fact was reported in many numerical and experimental studies (see, e.g., [14–18,20,31,32]).

Numerical and experimental data of [31] on the distribution of kinetic turbulence energy over the pipe radius for various concentrations of glass particles are compared in Fig. 3. The experimental conditions in these experiments

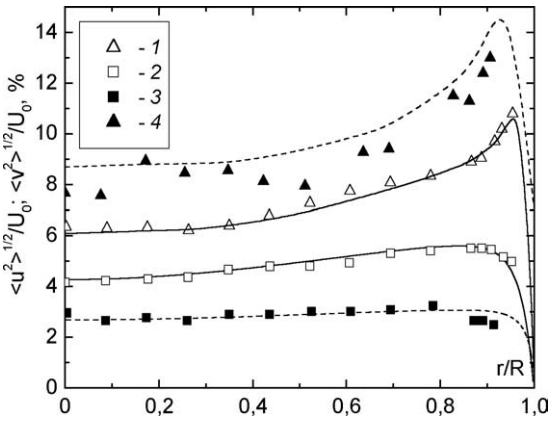

Fig. 2. Comparison of numerical results with the experimental data of Varaksin [31] on the distribution of root-mean-square pulsations of air and glass-particle velocities: (1) $\langle u^2 \rangle^{1/2}/U_0$; (2) $\langle v^2 \rangle^{1/2}/U_0$; (3) $\langle v_L^2 \rangle^{1/2}/U_0$; (4) $\langle u_L^2 \rangle^{1/2}/U_0$. Curves—calculation.

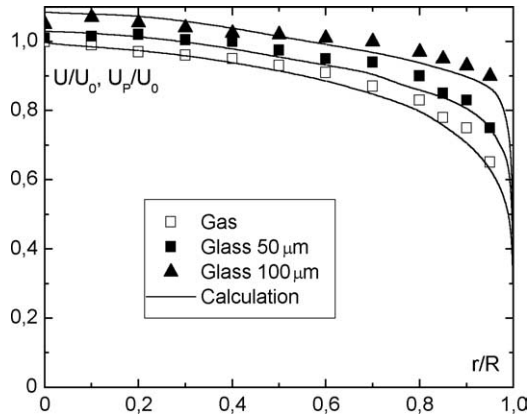

Fig. 1. Radial distributions of measured [31] and theoretically predicted glass-particle velocities in the stabilized flow.

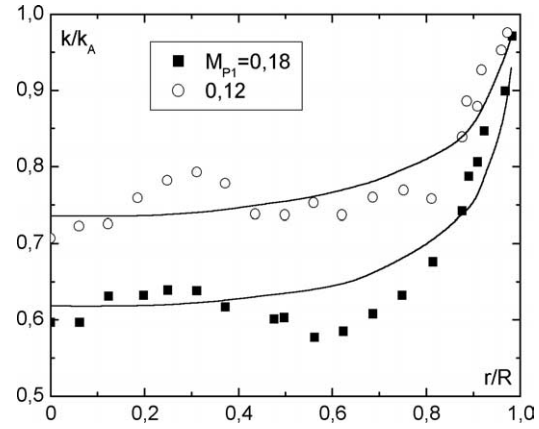

Fig. 3. Effect of particles on the distribution of gas-phase turbulence energy over the pipe cross-section. Curves—calculation, points—experiment [31].

corresponded to the following values of governing parameters: $2R = 64$ mm, $U_0 = 6.4$ m·s^{-1}, $d = 50$ μm, $\rho_p = 2550$ kg·m^{-3}, $\tau_+ = 20$, and $Re = 25\,600$. It is seen from Fig. 3 that the presence of relatively small particles in the flow suppresses the turbulence. The laminarizing action of the particles becomes more pronounced with increase in their mass concentration and with moving farther from the wall. These conclusions are also in line with the experimental data of [32].

Fig. 4 gives a comparison of predicted deposition rates of particles with the experimental data of Sehmel [33]. With increasing mass-mean flow velocity U_m, the rate of particle deposition onto the wall also increases; this regularity can be attributed to the intensifying effect of turbulent migration on the rate of particle deposition. It is seen from the figure that the calculation data for small particles ($d_1 < 0.1$ μm) display almost zero effect of the initial particle size on the deposition rate V_{LW}. This is caused by the limitation of the model since, in the submicrometer region, the transport of dispersed impurities is controlled by Brownian diffusion.

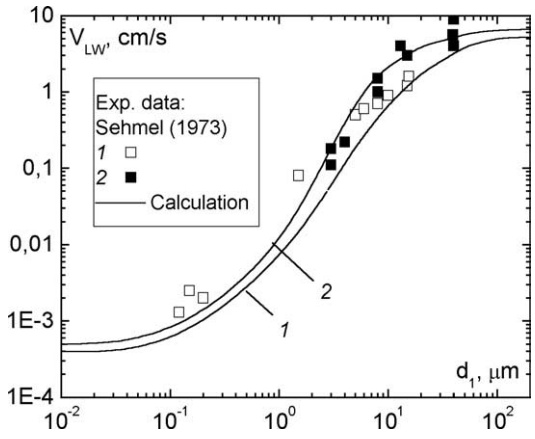

Fig. 4. Rate of particle deposition from the two-phase flow onto the duct wall versus the drop size. (1) $Re = 2 \times 10^5$; (2) $Re = 5 \times 10^5$.

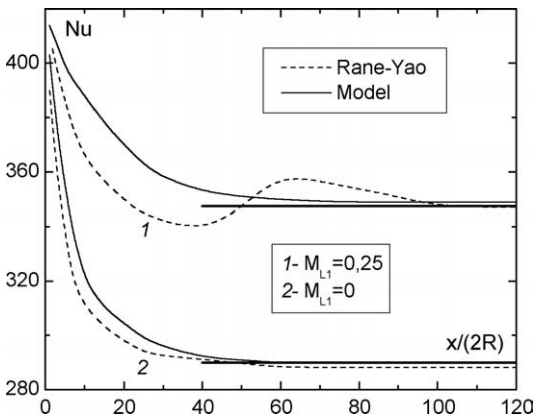

Fig. 5. Comparison of calculation results with the numerical data of [4] on the heat transfer in the turbulent vapor–drop flow. $Re_1 = 1.6 \times 10^5$.

6.3. Two-phase vapor–drop flow with heat transfer

The adequacy of the developed model for the single-component water–vapor flow under drop evaporation was checked by comparing its results with the numerical heat-transfer data of [4] obtained for a turbulent steady-state vapor–drop flow (see Fig. 5). A satisfactory agreement between the values predicted by the model and the data of Rane and Yao [4] was obtained.

7. Numerical results and comparison with experimental data

7.1. Numerical data

All calculations were performed for an air–water–vapor mixture with water drops. The pressure was atmospheric. The pipe length was 2 m, and the inner pipe diameter was 0.02 m. The values and ranges of initial parameters were as follows: the temperature of the steam-gas mixture at the inlet to the duct $T_1 = 293$ K; the drop temperature $T_{L1} = T_S = 293$ K; the initial drop diameter $d_1 = 0.1$–100 μm, which corresponded to the dimensionless time of particle relaxation $\tau_+ = 10^{-3}$–10^3; the flow Reynolds number $Re = U_1 2R/\nu = 10^4$–10^6; the particle Reynolds number calculated from the inter-phase velocity and from the initial dispersed-phase size $Re_P = d_1(\vec{U} - \vec{U}_L)/\nu = 0.01$–$4$ (thus, here we still remain in the Oseen flow mode region); the mass concentration of the drop phase $M_{L1} = 0$–0.1; and the mass fraction of water vapor $M_{V1} = 0.014$. Above, T_S is the equilibrium temperature under the adopted physical conditions. All calculations were performed assuming the condition of heat-flux constancy at the wall surface, $q_W = \text{const}$; the wall heat-flux density was $q_W = 5$ kW·m^{-2}.

The distributions of the dimensionless temperature $\Theta = (T_W - T)/(T_W - T_0)$ over the duct cross-section calculated for various mass concentrations of liquid drops are shown in Fig. 6. Curve 1 shows the temperature profile for the single-

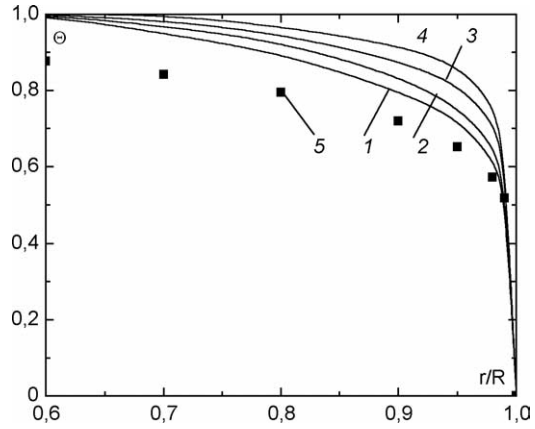

Fig. 6. Radial profiles of the temperature of the vapor–gas mixture. $Re = 13\,000$, $x/(2R) = 20$, $T_1 = T_{L1} = T_S = 293$ K, $d_1 = 30$ μm, $q_W = 5$ kW·m^{-2}. (1) $M_{L1} = 0$; (2) 0.01; (3) 0.05; (4) 0.1; (5) $\Theta = (1 - r/R)^{1/7}$.

phase air flow, and curve 5 was calculated by the classical "law of 1/7" for the region of stabilized flow. As is seen from the figure, an increase in the inlet concentration of liquid drops gives rise to more filled temperature profiles, thus intensifying the heat transfer to the pipe wall. The greater filling of the temperature profiles is caused, first of all, by higher intensity of evaporation processes in steam-gas flows with high air content. As the air concentration in the mixture increases, the diffusion flux of vapor from the surface of drops increases, resulting in a higher rate of drop evaporation.

The processes of heat and mass transfer between the liquid phase and the vapor–gas mixture, and also the heat transfer with the pipe surface are interrelated processes. To gain a better insight into the mechanism of these processes, it is required to examine the downstream evolution of the vapor-concentration fields. Such data are shown in Fig. 7. Note that, in the treated range of drop concentrations, the duct wall at the point $x/(2R) = 20$ still remains dry. The mass vapor content in individual cross-sections of the duct steadily increases (by several times) and attains its highest in the near-wall region, where the evaporation rate is maximal. The following feature in the figure deserves mention. Near the wall, where drops undergo rapid evaporation, the mass concentration of vapor displays a slight decrease. This fact can be explained by redistribution of the vapor concentration, which tends to acquire its initial profile. Fig. 7 shows that the distribution of the drop and steam concentration across the boundary layer displays rather a complex behavior.

Fig. 8 shows the radial distribution of the axial gas-phase velocity; here, U_0 is the velocity of the steam-gas flow at the pipe axis. An increase in the mass concentration of the dispersed phase gives rise to more filled velocity profiles, as well as to more filled temperature profiles of the vapor–gas mixture (see Fig. 6). The latter is caused by higher intensity of evaporation processes near the duct wall, by greater variation of the density of the two-phase flow in this region, and, hence, by the growth by the longitudinal pressure gradient. This is seen most clearly from the gas-phase velocity profile in the near-wall region, where, as the mass concentration of liquid drops ($M_{L1} > 5\%$) increases due to their evaporation, local maximum of the velocity of the vapor–gas flow appear. Note that calculations according to the full system of Euler equations (1)–(16) (see Fig. 8) show no notable changes in the gas-phase velocity data compared to the data predicted by the model of [9].

The distributions of the kinetic energy of gas-phase turbulence over the duct cross-section for various concentrations of liquid drops are shown in Fig. 9. As the surface is approached, the turbulence intensity increases due to the decrease of drop sizes in the course of evaporation and due to the rise of turbulence intensity in the near-wall zone. The decrease in the level of the turbulence kinetic energy is caused by active entrainment of relatively small particles into the pulsational motion of the gas phase and by transfer of pulsational energy from the vapor–gas mixture to liquid drops. These conclusions are in qualitative agreement with the experimental data of Tsuji et al. [32], who observed a slight increase in the turbulence level of the flow after adding large particles ($d_P = 3$ mm) to it and a dramatic decrease in the

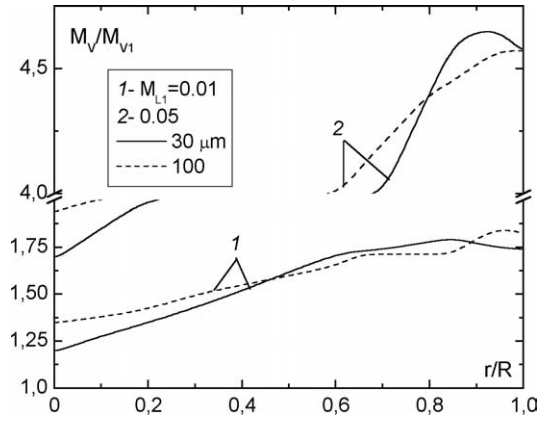

Fig. 7. Profiles of vapor concentration over the duct cross-section. The experimental conditions are the same as in Fig. 6. (1) $M_{L1} = 0.01$; (2) 0.05. Solid curves—$d_1 = 30$ μm; dashed curves—100 μm.

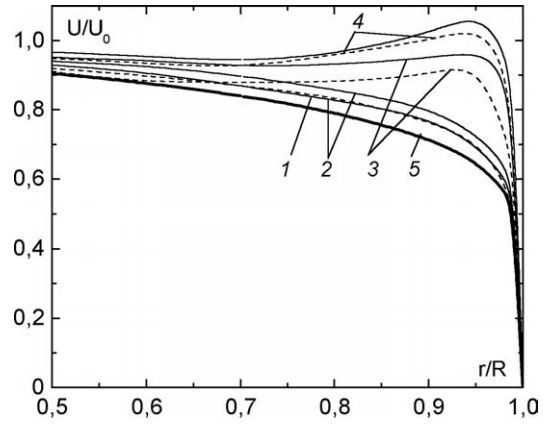

Fig. 8. Radial profiles of the velocity of the gas-phase mixture. (1) $M_{L1} = 0$; (2) 0.01; (3) 0.05; (4) 0.1; (5) $U/U_0 = (1 - r/R)^{1/7}$. Solid curves—calculation by the present model; dashed curves—calculation by the model of Terekhov and Pakhomov [9].

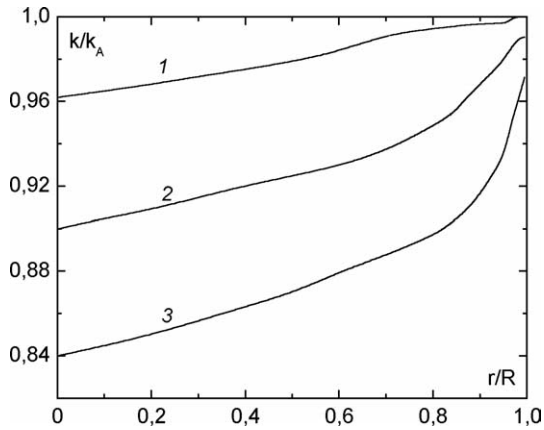

Fig. 9. Distribution of gas-phase turbulence energy in the gas–drop flow over the duct cross-section. (1) $M_{L1} = 0.01$; (2) 0.015; (3) 0.1.

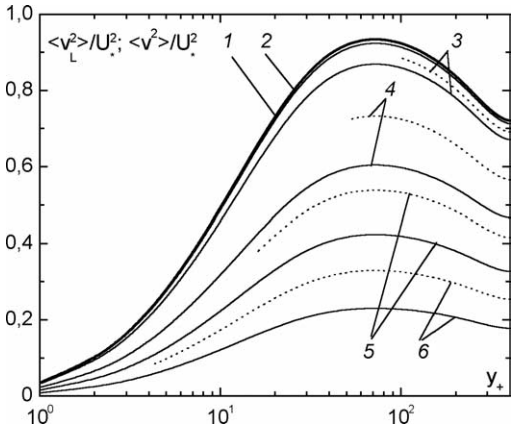

Fig. 10. Distribution of radial root–mean–square pulsations of the gas-phase and dispersed-phase velocities. (1) $\langle v^2\rangle^{1/2}/U_*^2$; (2)–(6) $\langle v_L^2\rangle^{1/2}/U_*^2$. (2) $d_1 = 1$ μm, $\tau_+ = 0.1$; (3) 10 μm, $\tau_+ = 8$; (4) 30 μm, $\tau_+ = 70$; (5) 50 μm, $\tau_+ = 190$; (6) 100 μm, $\tau_+ = 760$. Solid curves—adiabatic flow; dashed curves—non-isothermal flow.

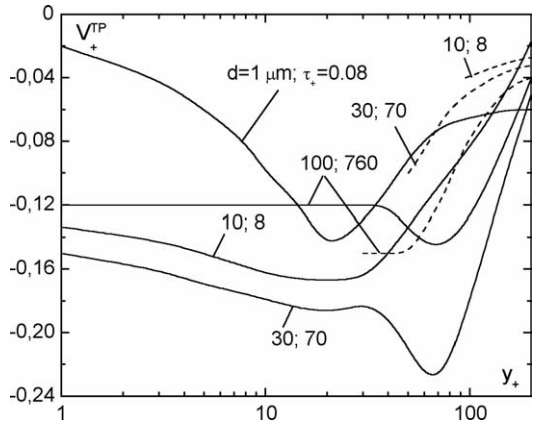

Fig. 11. Radial profiles of dimensionless turbophoresis velocity V_+^{TP}. Solid curves—adiabatic flow; dashed curves—non-isothermal flow.

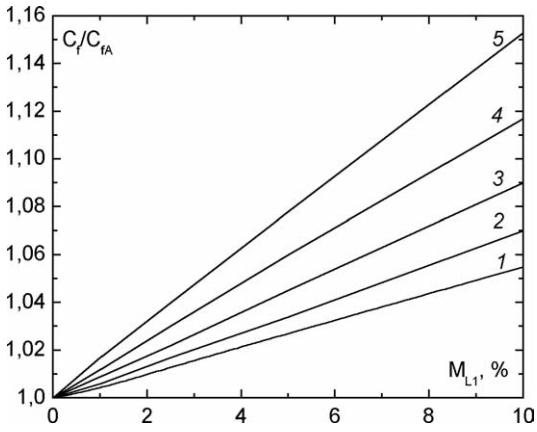

Fig. 12. Surface friction coefficient C_f/C_{fA} versus the mass concentration of the liquid phase. (1) $d_1 = 1$ μm, $\tau_+ = 0.1$; (2) $d_1 = 10$, $\tau_+ = 8$; (3) $d_1 = 30$, $\tau_+ = 70$; (4) $d_1 = 50$, $\tau_+ = 190$; (5) $d_1 = 100$, $\tau_+ = 760$.

turbulence kinetic energy after seeding the flow with small particles ($d_P = 200$ μm) or after decreasing their density (from $\rho_P = 2600$ kg·m^{-3} to $\rho_P = 1000$ kg·m^{-3}). Simultaneously, a third factor, the acceleration of high-inertia particles by the flow, may exert a more pronounced action, finally resulting in a growth of friction with increasing drop diameter.

The distributions of root-mean-square radial pulsations of the gas-phase and dispersed-phase velocities over the transverse coordinate for the cases of adiabatic ($q_W = 0$ kW·m^{-2}) and non-isothermal ($q_W = 5$ kW·m^{-2}) flows are shown in Fig. 10. The amplitude of these pulsations increases with distance from the wall due to the decrease of the mixing length and increase of the Stokes number $Stk = \tau/\Omega^L$, where Ω^L is the Lagrange integral time macroscale of turbulence, in the large-scale pulsational motion. As the drop size (or the dynamic-relaxation time τ of drops) increases, the drops get entrained into the large-scale high-energy pulsational motion of the gas phase; as a result, they can take off considerable turbulent energy from the gas flow. This effect becomes more pronounced with increasing number of drops. A decrease in the amplitude of air-velocity pulsations leads to a decrease of the intensity of dispersed-phase velocity pulsations. These data are in qualitative agreement with the data obtained for air flow with solid particles in a tube (see, e.g., [17,32]). The non-uniform distribution of temperature in the flow results in drop evaporation; accordingly, the drop size and the mass concentration of liquid drop decrease, and the drops take off lesser amount of the gas-phase turbulent energy after being involved into the pulsational motion.

The non-uniformity of radial drop-velocity pulsations causes migration of liquid drops in the direction along which the intensity of dispersed-phase pulsations decreases. Fig. 11 shows the distribution of the relative turbophoresis velocity $V_+^{TP} = V^{TP}/U_* = -\tau_+ \partial\langle v_{L+}^2\rangle/\partial r_+$ over the duct cross-section for drops of various sizes (here, the sign "+" shows that the marked quantity is written in dynamic variables). The dashed and solid curves in this figure refer to non-isothermal turbulent gas–drop flow ($q_W = 5$ kW·m^{-2}) and to adiabatic turbulent gas–drop flow ($q_W = 0$ kW·m^{-2}). The velocity of migrating drops is directed towards the duct wall; it substantially depends on the particle size and on the transverse coordinate. An increase in the initial drop size (or in the dynamic-relaxation time) causes a rise of the turbophoresis velocity due to the increasing role of turbulent dispersion-phase transfer mechanisms. As the drop size further increases, the turbulent-migration velocity decreases due to flattening of the distribution of particle-velocity pulsations over the duct cross-section.

Fig. 12 illustrates the effect of the mass content of liquid drops in the flow in the surface-friction coefficient. Here, C_{fA} is the surface friction coefficient for the single-phase air flow. The friction coefficient almost linearly increases with increasing drop concentration and with increasing drop size. Nevertheless, this increase is insignificant, amounting to about 15% for the mass concentration of large drops $M_{L1} = 0.1$. Another important feature of Fig. 12, which is worth noting, is that, with increasing drop diameter, the

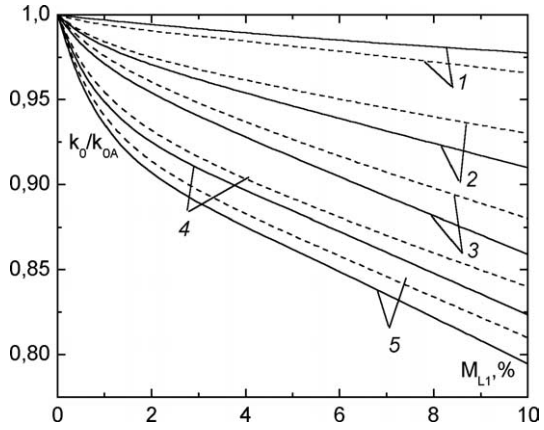

Fig. 13. Radial profiles of the kinetic energy k_0/k_{0A} of the gas-phase turbulence. The designations are the same as in Fig. 12. Solid curves—calculation by the present model; dashed curves—calculation by the model of [9].

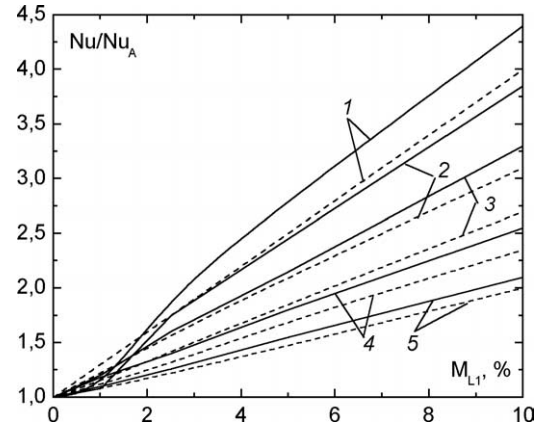

Fig. 14. Variation of the heat transfer intensification ratio Nu/Nu_A in the gas–drop flow. The designations are the same as in Fig. 12. Solid curves—calculation by the present model; dashed curves—calculation by the model of [9].

friction coefficient also increases. The downstream evolution of the axial-velocity profiles (see Fig. 8) and, hence, the variation of the friction coefficient in the steamwise direction is influenced by many factors.

The presence of the dispersed phase in the flow suppresses the gas-phase turbulent pulsations. This is evident from the numerical data of Fig. 13 (here, k_{0A} is the kinetic energy of air turbulence at the pipe axis); these data show that large drops and their high concentration promote flow laminarization due to entrainment of liquid drops into the high-energy large-scale vortices of the gas flow. Very small drops turbulize the flow since they suppress viscous dissipation in the equation for the gas-turbulence kinetic energy [18]. Calculations by the full system of Euler equations (see Fig. 13) yield no considerable changes in the results concerning the kinetic energy of the gas-phase turbulence compared to the data obtained by the model of Terekhov and Pakhomov [9]. The latter shows that non-uniformities in the drop-concentration fields and in the average inter-phase velocity only insignificantly affect the values of k and ε. For this reason, in the first-order approximation, these terms can be omitted from Eq. (3).

Fig. 14 illustrates the effect of mass content of liquid drops on the heat-transfer intensification ratio. In this figure, Nu_A is the Nusselt number in a single-phase air flow with the identical flow Reynolds number. As is seen from Fig. 14, the presence of evaporating drops exerts a profound influence on the heat-transfer intensification ratio in the two-phase gas–drop flow (the heat-transfer rate increases more than threefold); simultaneously, the wall friction increases insignificantly, approximately by 15% (see Fig. 12). The greater the drop diameter, the higher is the surface friction; on the contrary, the heat-transfer rate decreases (see Fig. 14). Calculations by the full system of equation in the Euler approximation of the Nusseldt number (see Fig. 14) yield considerable changes in the calculated values of *Nu* compared to the data obtained by the model of [9]. Thus, it is the rate of heat transfer between the duct wall and the gas phase that is affected

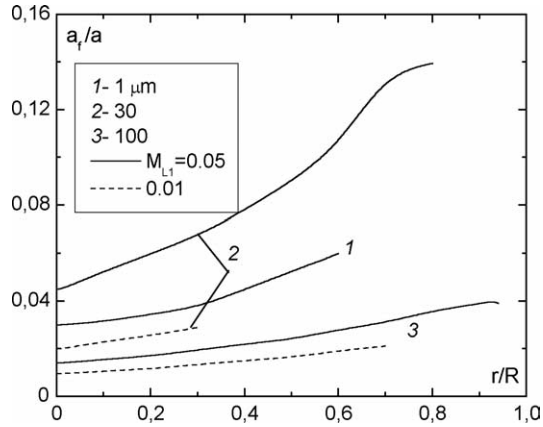

Fig. 15. Distribution of the radial drop acceleration over the tube cross-section.

by the pulsations of velocity and temperature of evaporating drops in a greater extent.

Fig. 15 shows the distributions of radial drop-acceleration ratios over the duct radius. Here, $a_f = \frac{\partial\langle v_L^2\rangle}{\partial r}$; $a = U_L\frac{\partial V_L}{\partial x} + \frac{V_L}{r}\frac{\partial(rV_L)}{\partial r}$. It should be noted that, with increase in the drop concentration and in the initial drop size, the value of the turbophoresis-induced radial acceleration decreases since the level of dispersed-phase velocity pulsations diminishes. Initially, as the drop diameter increases, the turbophoresis-induced acceleration increases because turbulent transport mechanisms start operating (submicrometer drops are transferred via Brownian diffusion); that is the reason for the growth of the turbophoresis-induced radial acceleration. Note that, under the adopted conditions, the migration transfer of liquid drops should necessarily be taken into account since it may give rise to considerable drop fluxes.

The distribution of turbulent heat fluxes in the dispersed phase over the duct cross-section is shown in Fig. 16, where $q_f = \frac{1}{r\Phi}\frac{\partial(r\Phi\langle\theta v_L\rangle)}{\partial r}$; $q = U_L\frac{\partial T_L}{\partial x} + \frac{V_L}{r}\frac{\partial(rT_L)}{\partial r}$. The turbulent heat fluxes supplying heat to liquid drops turned out to

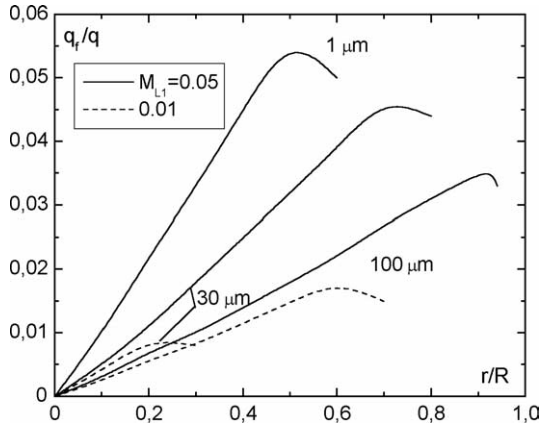

Fig. 16. Radial distribution of the turbulent heat flux in the dispersed phase.

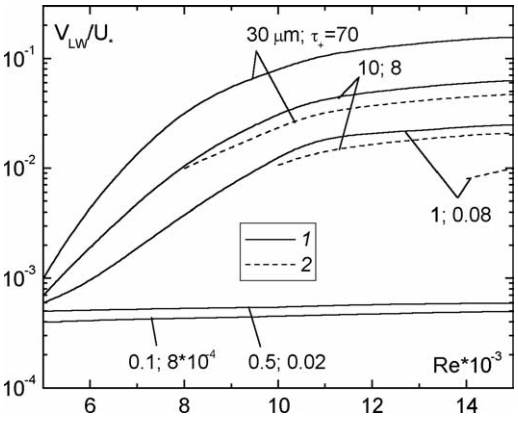

Fig. 17. Dimensionless rate of drop deposition versus the flow Reynolds number in the isothermal and non-isothermal flows. (1) $q_W = 0$ kW·m^{-2}; (2) 5.

be lesser than the radial accelerations in Fig. 15; for this reason, in the first-order approximation, the term q_f can be neglected compared to q. An increase in the liquid-phase concentration causes an increase in the fraction of the turbulent heat flux that supply heat to liquid drops because more drops get entrained into the high-energy gas-velocity and gas-temperature pulsations and due to transfer of heat in the radial direction by the stochastic motion of liquid drops.

The relative rates of dispersed phase deposition from the turbulent gas–drop flow onto the duct wall in the cases of adiabatic ($q_W = 0$ kW·m^{-2}) and non-isothermal ($q_W = 5$ kW·m^{-2}) flows are shown in Fig. 17 as a function of the flow Reynolds number $Re = U_1 2R/\nu$. With increasing Reynolds number, the deposition rate also increases, which can be explained by the increasing role of turbulence-related processes, namely, diffusion and turbophoresis. It is seen from the figure that the deposition rate of submicrometer drops is practically independent of the *Re* number since, here, it is Brownian diffusion that plays a predominant part. The heat transfer is related with drop evaporation and, hence, with the reduction of drop sizes; that is why the rate of drop deposition diminishes as drops undergo evaporation.

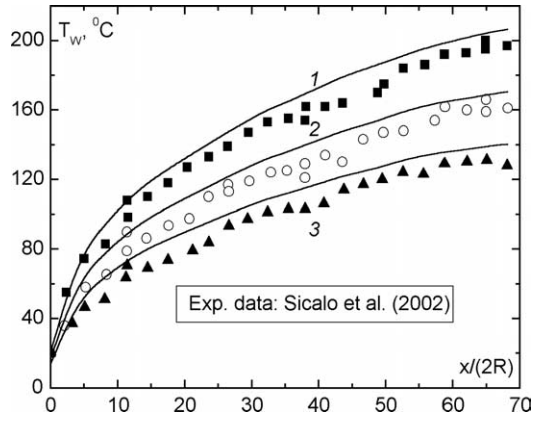

Fig. 18. Variation of the wall temperature. Curves—calculation; points—experimental data of [11]. (1) $q_W = 17.84$ kW·m^{-2}; (2) 13.92; (3) 11.5.

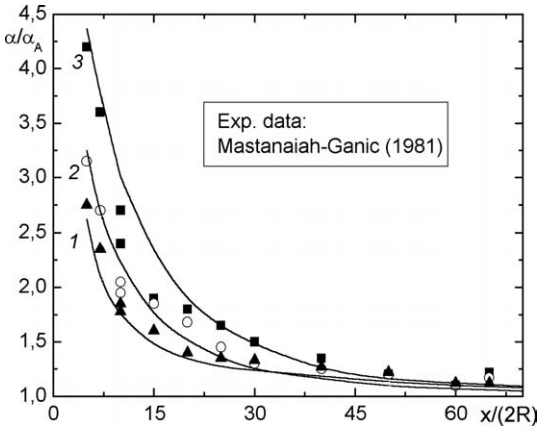

Fig. 19. Heat transfer intensification ratios as predicted by the present model in comparison with the experimental data of Mastanaiah and Ganic [3] and numerical data of our study. (1) $q_W = 14.53$ kW·m^{-2}; (2) 8.34; (3) 6.4.

Results similar to those shown in Fig. 15–17 were also obtained for other proportions of inlet parameters.

7.2. Comparison with the experimental data

Subsequent figures compare the present calculation results with previously reported experimental data on heat and mass transfer in ducted stabilized flows.

The longitudinal distributions of the wall temperature T_W measured by Sicalo et al. [12] are shown in Fig. 18. The initial data for performing the comparative analysis were: $M_{L1} = 0.5\%$, $Re = U_1 2R/\nu = 39\,300$, $2R = 13.2$ mm, calculation length 0.924 m, $G_A = 7.58$ g·s^{-1}, $d_1 = 16$ μm, $\tau_+ = 272$, and $T_1 = 293$ K. The experiments were carried out under atmospheric pressure. The data of Fig. 12 show that the predicted distributions of the wall temperature compare well with the measured ones.

The heat-transfer intensification ratios measured by Mastanaiah and Ganic [3] and the heat-transfer intensification ratios predicted by the present model are compared in Fig. 19, where the quantity α_A corresponds to the case of a

single-phase air flow under identical conditions. The initial data in the numerical experiment were: $M_{L1} = 1.1$–2.1%, $Re = U_1 2R/\nu = 21\,800$–$58\,600$, $2R = 12.95$ mm, calculation length 0.889 m, $G_A = 4.02$–10.8 g·s^{-1}, $d_1 = 9$–23 μm, $\tau_+ = 139$–208, and $T_1 = 300$ K. The experiments were carried out under atmospheric pressure. Both measured and predicted α/α_A ratios display a monotonic decrease over the duct length and reduction with increasing wall heat-flux density. An increase in the wall heat-flux density causes a decrease in the heat-transfer ratio because, in this case, the wall temperature rises.

8. Conclusions

We developed a physical model of combined heat and mass transfer in the turbulent flow of a gas–drop mixture. This model treats the liquid phase as local sinks of heat and sources of vapor mass and inter-phase friction. To calculate turbulent characteristics of the gas phase, we used the LRN k–ε model of Nagano and Tagawa, extended to the case of a flow with a dispersed phase. A closed system of transfer equations for the gas and dispersed phases, based on using the Euler approach, is constructed. The model takes into account the deposition of liquid drops onto the wall, the heat transfer caused by direct contacts of drops with the wall, and the turbulent migration of the dispersed phase.

An increase in the mass concentration of liquid drops leads to a considerable (by several times) intensification of heat- and mass-transfer processes in the two-phase flow, with a corresponding growth of the fraction of the heat spent on the phase transition and on the heat transfer due to drop contacts with the wall.

An increase in the initial drop diameter leads to a dramatic decrease in the rate of heat transfer between the duct wall and the gas–vapor–drop mixture; simultaneously, the wall friction increases insignificantly. The distribution of the concentration of components of the two-phase mixture over the duct cross-section displays a complex downstream behavior. As the drop concentration increases, a local maximum appears in the gas-phase velocity profile; this maximum, caused by the evaporation of the dispersed phase, lies in the near-wall zone.

The calculations treating the gas and dispersed phases in the Euler approximation yield substantial differences in the results concerning the heat transfer and turbulence of the gas and drop phases due to more adequate description of interphase transfer as compared to the model of Terekhov and Pakhomov [9].

Acknowledgements

This work was supported by the Russian Foundation for Basic Research (Grant No. 01-02-16994) and by the Russian Federation's Presidental Foundation for Leading Scientific Schools (Grant No. 1308.2003.8). The authors express their gratitude to Prof. I.V. Derevich (Moscow State University of Environmental Engineering) and L.I. Zaichik (High Temperature Institute RAS, Moscow) for fruitful discussion. Authors also thank Prof. A.Yu. Varaksin (High Temperature Institute RAS, Moscow) for experimental data for turbulent gas-particle flow leaved to electronic form.

References

[1] K. Hishida, M. Maeda, S. Ikai, Heat transfer from a flat plate in two-component mist flow, ASME J. Heat Transfer 102 (1980) 513–518.
[2] V.I. Terekhov, M.A. Pakhomov, Numerical study of heat transfer in a laminar mist flow over a isothermal flat plate, Internat. J. Heat Mass Transfer 45 (2002) 2077–2085.
[3] K. Mastanaiah, E.N. Ganic, Heat transfer in two-component dispersed flow, ASME J. Heat Transfer 103 (1981) 300–306.
[4] A.G. Rane, S.-Ch. Yao, Convective heat transfer to turbulent droplet flow in circular tubes, ASME J. Heat Transfer 103 (1981) 679–684.
[5] A.I. Leont'ev, Propagation of limiting laws of friction and heat transfer on a turbulent stream regimes of a gas/liquid flows, Proc. Siberian Division of Academy Sciences of USSR. Ser. Technical Sciences 10 (1984) 47–58.
[6] A. Berlemont, M.S. Grancher, G. Gouesbet, Heat and mass transfer coupling between vaporizing droplets and turbulence using Lagrangian approach, Internat. J. Heat Mass Transfer 38 (1995) 3023–3034.
[7] X. Li, J.L. Gaddis, T. Wang, Modeling heat transfer in a mist/steam impinging jet, ASME J. Heat Transfer 123 (2001) 1086–1092.
[8] V.I. Terekhov, M.A. Pakhomov, A.V. Chichindaev, Heat and mass transfer in the developed turbulent two-component gas–vapor and droplet flow, J. Engrg. Phys. Thermophys. 74 (2001) 331–338.
[9] V.I. Terekhov, M.A. Pakhomov, Numerical simulation of hydrodynamics and convective heat transfer in turbulent tube mist flow, Internat. J. Heat Mass Transfer 46 (2003) 1503–1517.
[10] C.T. Crowe, M.P. Sharma, D.E. Stock, The Particle-Source-In-Cell (PSI-Cell) model for gas–droplet flows, ASME J. Fluid Engrg. 99 (1977) 325–332.
[11] A.A. Mostafa, S.E. Elghobashi, A two-equation turbulence model for jet flow with vaporizing droplets, Internat. J. Multiphase Flow 11 (1985) 515–534.
[12] S. Sikalo, N. Delalic, E.N. Ganic, Hydrodynamics and heat transfer investigation of air–water dispersed flow, Internat. J. Exp. Thermal Fluid Sci. 25 (2002) 511–521.
[13] I.N. Gusev, E.I. Guseva, L.I. Zaichik, Deposition of particle on channel walls in a turbulent flow, J. Engrg. Phys. Thermophys. 59 (1990) 735–742 (in Russian).
[14] A.A. Shraiber, L.B. Gavin, V.A. Naumov, V.P. Yatsenko, Turbulent Flows in Gas Suspensions, Hemisphere, New York, 1990.
[15] R.I. Nigmatulin, Dynamics of Multiphase Media, Hemisphere, New York, 1991.
[16] E.P. Volkov, L.I. Zaichik, V.A. Pershukov, Numerical Modeling of Combustion of Solid Fuel, Nauka, Moscow, 1994 (in Russian).
[17] I.V. Derevich, The hydrodynamics and heat transfer and mass transfer of particles under conditions of turbulent flow of gas suspension in a pipe and in an axisymmetric jet, High Temperature 40 (2002) 78–91.
[18] I.V. Derevich, L.I. Zaichik, The particle deposition from the turbulent flow, Fluid Dynamics 23 (1988) 96–104 (in Russian).
[19] Y. Nagano, M. Tagawa, An improved (k–ε) model for boundary layer flow, ASME J. Fluids Engrg. 109 (1990) 33–39.
[20] W.S.J. Uijetterwaal, R.V.A. Oliemans, Particle dispersion and deposition in direct numerical and large eddy simulations of vertical pipe flow, Phys. Fluids A 8 (1996) 2590–2604.

[21] I.V. Derevich, R.S. Gromadskaya, Simulation of particle deposition from a turbulent two-phase flow, Theoret. Found. Chem. Engrg. 32 (1998) 260–265.

[22] A.I. Leont'ev, Engineering methods for calculation of friction and heat transfer on permeable surface, Heat Engrg. 9 (1972) 19–24 (in Russian).

[23] M.C. Yuen, L.W. Chen, Heat transfer measurements of evaporating liquid droplets, Internat. J. Heat Mass Transfer 21 (1978) 537–542.

[24] E.N. Ganic, W.M. Rohsenow, On the mechanism of liquid drop deposition in two-phase dispersed flow, ASME J. Heat Transfer 101 (1979) 288–294.

[25] O. Simonin, Q. Wang, K.D. Squires, Comparison between two-fluid model predictions and large eddy simulation results in a vertical gas-solid turbulent channel flow, in: ASME Fluids Engrg. Division Summer Meeting. FEDSM '97-3625, 1997, pp. 1–10.

[26] K.-C. Chang, M.-J. Shyu, Revisiting the Reynolds-averaged energy equation in near-wall turbulence model, Internat. J. Heat Mass Transfer 43 (2000) 665–676.

[27] D.A. Anderson, J.C. Tannehill, R.H. Pletcher, Computational Fluid Mechanics and Heat Transfer, Hemisphere, New York, 1984.

[28] J.G.M. Eggels, F. Unger, M.H. Weiss, J. Westerweel, R.J. Adrian, R. Friedrich, F.T.M. Nieuwstadt, Fully developed pipe flow: A comparison between direct numerical simulation and experiment, J. Fluid Mech. 268 (1994) 175–209.

[29] S.S. Kutateladze, A.I. Leont'ev, Heat and Mass Transfer and Friction in Turbulent Boundary Layer, Hemisphere, New York, 1989.

[30] S.I. Isaev, et al., in: A.I. Leont'ev (Ed.), Theory of Heat and Mass Transfer, Publishing House of Bauman Moscow State Technical University, Moscow, 1997 (in Russian).

[31] A.Yu. Varaksin, Turbulent Gas Flows With Solid Particles, Internat. Academic Publishing Company Nauka, Moscow, 2003 p. 192 (in Russian).

[32] Y. Tsuji, Y. Morikawa, H. Shiomi, LDV measurements of an air-solid two-phase flow in a vertical pipe, J. Fluid Mech. 139 (1984) 417–434.

[33] G.A. Sehmel, Particle eddy diffusivities and deposition velocities for isothermal flow and smooth surfaces, J. Aerosol. Sci. 4 (1973) 125–138.